ADVANCED MATERIALS
www.advmat.de

www.MaterialsViews.com

X-Space MPI: Magnetic Nanoparticles for Safe Medical Imaging

Patrick William Goodwill, Emine Ulku Saritas, Laura Rose Croft, Tyson N. Kim, Kannan M. Krishnan, David V. Schaffer, and Steven M. Conolly*

One quarter of all iodinated contrast X-ray clinical imaging studies are now performed on Chronic Kidney Disease (CKD) patients. Unfortunately, the iodine contrast agent used in X-ray is often toxic to CKD patients' weak kidneys, leading to significant morbidity and mortality. Hence, we are pioneering a new medical imaging method, called Magnetic Particle Imaging (MPI), to replace X-ray and CT iodinated angiography, especially for CKD patients. MPI uses magnetic nanoparticle contrast agents that are much safer than iodine for CKD patients. MPI already offers superb contrast and extraordinary sensitivity. The iron oxide nanoparticle tracers required for MPI are also used in MRI, and some are already approved for human use, but the contrast agents are far more effective at illuminating blood vessels when used in the MPI modality. We have recently developed a systems theoretic framework for MPI called x-space MPI, which has already dramatically improved the speed and robustness of MPI image reconstruction. X-space MPI has allowed us to optimize the hardware for five MPI scanners. Moreover, x-space MPI provides a powerful framework for optimizing the size and magnetic properties of the iron oxide nanoparticle tracers used in MPI. Currently MPI nanoparticles have diameters in the 10-20 nanometer range, enabling millimeter-scale resolution in small animals. X-space MPI theory predicts that larger nanoparticles could enable up to 250 micrometer resolution imaging, which would represent a major breakthrough in safe imaging for CKD patients.

1. Introduction

Magnetic Particle Imaging (MPI) is an imaging modality that maps the in vivo spatial distribution of magnetic nanoparticle contrast agents.[1–6] The technique shows extraordinary promise as a safe substitute for iodinated or gadolinium contrast angiograms in patients with poor kidney function who have difficulty excreting these standard contrast agents. First introduced in 2005 by Gleich and Weizenecker,[1] the technique exploits the nonlinear magnetization characteristics of superparamagnetic iron oxide (SPIO) nanoparticles to localize the spatial position of the nanoparticles. The resolution and sensitivity of MPI are governed by the nanoparticle characteristics and by the strength of the applied magnetic field gradient, so materials scientists can make critical and foundational contributions to this new imaging modality. It is interesting that, like Magnetic Resonance Imaging (MRI), the spatial resolution of MPI is orders of magnitude finer than the wavelength of the electromagnetic fields used to interrogate the magnetic nanoparticles. MPI excitation frequencies are typically below 25 kHz, which corresponds to a wavelength in the body of about 1 kilometer. MPI resolution, on the other hand, can be more than 6 orders of magnitude finer than the wavelength and is measured in millimeters.

MPI is perhaps the first imaging technique designed around a tracer, rather than developing a tracer to work with an existing imaging technique. Human tissue is diamagnetic, so it manifests zero MPI signal. This means MPI images have near-perfect contrast, with no obscuring background tissue. Also, with low-frequency magnetic fields, there is zero depth attenuation, meaning the MPI scan is quantitative at any depth. MPI's superb contrast is a major advantage over today's standard angiography techniques, X-ray, CT and MRI angiography. It is worth noting that catheterized arterial injections are commonly used in X-ray angiography only because this increases the concentration of the iodinated contrast about 30-fold over much safer venous injections. The risky catheterized arterial delivery is essential to overcoming the inherently low X-ray image contrast between tiny blood vessels and background tissues. Since tissue is transparent to magnetic fields and MPI

Dr. P. W. Goodwill, Dr. E. U. Saritas, L. R. Croft, T. N Kim
Department of Bioengineering
University of California
Berkeley, Berkeley, CA 94720-1762 USA
E-mail: goodwill@berkeley.edu
Prof. S. M. Conolly
Departments of Bioengineering and EECS
University of California
Berkeley, Berkeley, CA 94720-1762 USA
Prof. D. V. Schaffer
Department of Chemical & Biomolecular Engineering
University of California
Berkeley, Berkeley, CA 94720-1462 USA
Prof. K. M. Krishnan
Departments of Materials Science & Physics
323 Roberts Hall, Box 352120
University of Washington
Seattle, WA 98195-2120 USA

DOI: 10.1002/adma.201200221

does not see tissue at all, MPI angiography could detect low concentrations of the nanoparticle tracer, allowing for much safer venous injections. MPI shares the excellent contrast of nuclear imaging, but with much finer spatial resolution, and with no ionizing radiation.

Patient safety is another important motivation for MPI angiography. All three existing techniques for angiography, planar X-ray angiography, CT angiography, and MR angiography, use Iodine or Gadolinium tracers that are hazardous for patients with Chronic Kidney Disease (CKD).[7–9] The X-ray contrast agent Iodine is the dominant tracer for clinical angiography; indeed, over 80 million iodinated contrast studies were administered in 2003 worldwide.[7] However, even a single iodine injection puts a CKD patient at risk for contrast-induced nephropathy (CIN).[7,8] Although rare (<1%), severe CIN can require dialysis and is associated with high in-hospital mortality (36%) and high two year mortality (81%).[8] The number of patients with CKD is growing rapidly due to comorbidity with Type II diabetes and high blood pressure as well as aging demographics.[7] Half of all American patients over the age of 70 have CKD, and one quarter of all X-ray angiography patients have CKD,[10] so iodinated contrast is a significant public health safety concern. We hope that MPI will soon offer a safer replacement for today's angiography methods because SPIO nanoparticles are much safer than iodine or gadolinium for CKD patients. Indeed, SPIOs have been used as a *treatment* for anemia in CKD patients.[11] Importantly, these iron oxide tracers are processed in the liver and do not affect the kidneys.[11]

Here we give a brief introduction to the MPI imaging method and explain how the fundamental image parameters, signal-to-noise ratio (SNR), contrast, and spatial resolution depend on the scanner hardware and the magnetic properties of the iron oxide imaging tracer. We include some of the first full-body mouse MPI images, and discuss promising future directions of magnetic particle imaging.

2. The MPI Imaging Process

The MPI technique (illustrated in **Figure 1**) relies on spatially selective saturation of magnetic nanoparticles inside an animal or patient. This spatially selective saturation is achieved by a strong magnetic field gradient, typically in the 2–8 T/m range. At the origin of the gradient there is a region, known as a Field Free Point (FFP), where the magnetic field magnitude is weaker than the saturation field of the SPIOs. For currently available SPIOs and 6 T/m gradients, the FFP is a millimeter-scale spheroid. In regions outside the FFP, all SPIOs are magnetically saturated and produce no signal in the receiver coil since the coil can only detect time-varying magnetizations. Within the FFP, SPIOs are not saturated and can produce an MPI signal. Imaging occurs as the FFP is rapidly shifted across the field-of-view (FOV), causing any SPIOs in the current voxel to flip 180°, inducing a voltage in the receiver coil. We can shift the FFP mechanically and/or electronically. Electronic shifting requires adding a time-varying *uniform* magnetic field.

After the raw MPI signal from the nanoparticles is picked up in the receiver coil, an MPI image can be reconstructed. The two principal methods for reconstructing an image in MPI are called harmonic-space MPI and x-space MPI. Both reconstruction algorithms are described below.

2.1. Harmonic-space MPI

The earliest image reconstruction technique for MPI is harmonic-space MPI, which relies on a system matrix to

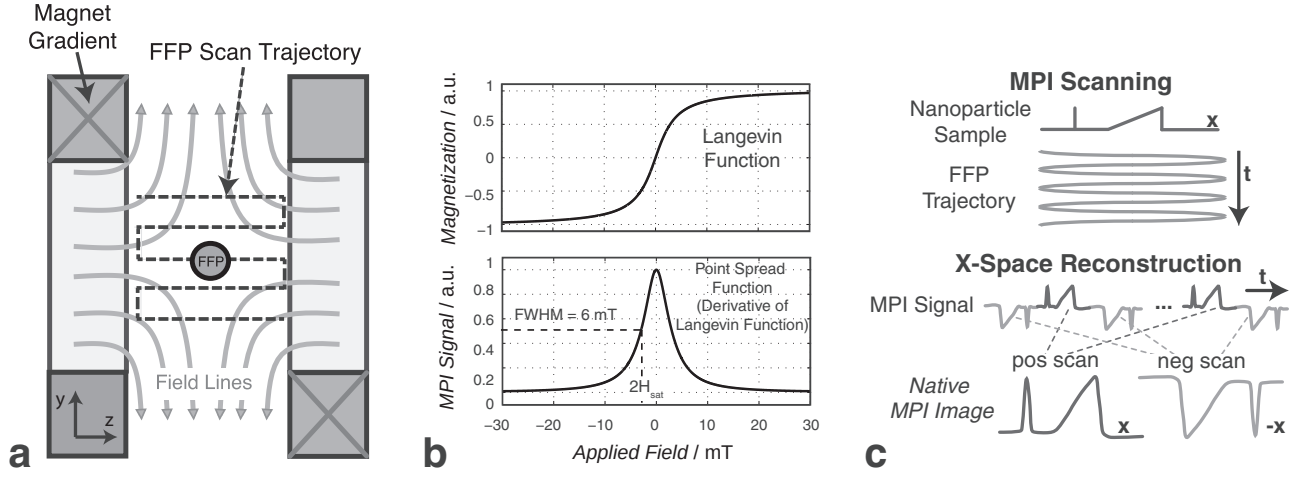

Figure 1. (a) A strong magnetic field gradient forms a sensitive point known as a Field Free Point (FFP). The FFP can be moved in a scan trajectory to cover the imaging field of view. (b) The magnetization of SPIOs demonstrate a nonlinear behavior as a function of the applied field, which can be modeled using a Langevin function. X-space MPI states that the Point Spread Function (PSF) in MPI is the derivative of this Langevin function. The simulated PSF is for a log-normally distributed iron oxide nanoparticle with diameter 20 +/– 2.5 nm, which has a FWHM of 6 mT. In a 6 T/m gradient field, this theoretical FWHM corresponds to 1 mm resolution. (c) When the FFP rapidly traverses a nanoparticle sample, the nanoparticles induce a signal in an inductive receive coil. X-space reconstruction involves gridding the instantaneous signal to the position of the FFP to form a native MPI image.

pre-characterize the signal response of the magnetic nanoparticles.[1,12,13] The system matrix stores the Fourier harmonics of an ideal MPI impulse response located at every possible location of a point source. The system matrix is typically measured physically with a nanoparticle sample.[12]

Once the system matrix is measured, reconstruction is achieved through matrix inversion techniques such as singular value decomposition. This inversion can be quite complex and ill-posed, since the system matrix is a dense matrix containing over a billion elements. For example, for an image with $N_x N_y N_z$ voxels, the system matrix size will be $N_c N_f \times N_x N_y N_z$ where N_c is the number of receive coils and N_f is the number of harmonics used in the reconstruction.[12] In particular, care must be taken when regularizing the solution to achieve high resolution while not amplifying noise when inverting the system matrix. It is important that MPI be subjected to well-conditioned image reconstruction to avoid any loss of SNR. Beyond the computational challenges, another challenge is robustness. If the pre-characterization scans do not precisely reproduce the tracer's in vivo micro-environment, then the reconstructed image may have artifacts. It is known that local viscosity as well as concentration can alter the MPI signal,[14] and that viscosity of blood varies between the major blood vessels and the microvasculature. These variations could produce modeling errors and lead to a less accurate system matrix, which would translate to imaging artifacts.

2.2. X-space MPI

We recently introduced the x-space reconstruction technique to improve both the robustness and the speed of MPI image reconstructions.[2,3] First we showed that MPI could be analyzed similarly to the powerful k-space theory of MRI.[15] The key difference is that the MPI signal represents a temporal scan through *x-space*, instead of the spatial-frequency domain. The raw MPI signal is then converted into an x-space MPI image using a very fast and robust two-step process of velocity compensation followed by gridding to the instantaneous position of the FFP. No matrix inversion or pre-characterization is required, and no modeling regarding the in vivo micro-environment is needed; hence, the x-space image reconstruction algorithm is robust and real-time.

X-space theory offers several advantages over harmonic-space reconstructions.[12] Specifically, x-space MPI offers experimentally proven Linearity and Shift Invariance (LSI), as well as real-time image reconstruction speed as it involves only velocity compensation and gridding. Importantly, x-space MPI makes no attempt to deconvolve the MPI signal to improve resolution over the native resolution determined by the physics of the nanoparticles and field gradient, and thus avoids the significant noise gain of deconvolution (see the noise gain in Knopp et al. 2011).[16]

X-space MPI theory requires three assumptions:[2,3] First, we can generate a strong magnetic field gradient and a uniform magnetic field (> 2.5 T/m) that define a unique FFP within the FOV (See Figure 1). Second, SPIOs can be instantaneously adiabatically aligned and saturated with an applied magnetic field greater than about 5 mT. Last, we assume that low-frequency MPI signals lost during signal detection (which must be filtered out to prevent direct feedthrough interference) are recoverable using robust signal processing methods.[17] The problem of lost low-frequency signals is not unique to x-space MPI; system matrix reconstruction must also account for the lost information.

In x-space MPI, we express the image as a convolution of the nanoparticle spatial distribution with the point spread function (PSF) of the system. The key result of this analysis is the signal equation in one dimension, which states that the MPI signal samples the real space convolution of a nanoparticle density $\rho(x)$ [particles/m^3] with a PSF $h(x)$ at the instantaneous location of the FFP $x_s(t)$

$$s(t) = B_1 m \rho(x) * h(x)\Big|_{x = x_s(t)} \frac{G\dot{x}_s(t)}{H_{sat}} \tag{1}$$

where the system PSF is determined both by the magnetization characteristics of the nanoparticles, as well as the magnetic field gradient. As shown in Figure 1(b), the magnetization of superparamagnetic nanoparticles is nonlinear and follows what is known as the Langevin function. The receiver coil only detects the change in the magnetization level, hence the PSF is the derivative of the Langevin function

$$h(x) = \dot{L}\left(\frac{Gx}{H_{sat}}\right) \tag{2}$$

This 1D PSF is similar to a Lorentzian function.[3] Note that the magnitude of the signal in Equation 1 changes with the sensitivity of the receive coil B_1 [T/A], the magnetic moment of a single magnetic nanoparticle in the tracer m [Am^2], the field required to half saturate a magnetic nanoparticle tracer H_{sat} [A/m], the gradient field strength G [A/m/m] and the FFP slew rate $x'_s(t)$ [m/s]. The product $Gx'_s(t)$ [A/m/s] is simply the slew rate of the field used to excite the sample.

Dividing out the slew rate of the excitation field and the various constants, we see that we can produce a native image in x-space

$$\hat{\rho}(x_s(t)) = \rho(x) * h(x)|_{x=x_s(t)} \tag{3}$$

Of great importance is the shape of the system PSF, $h(x)$, which defines the native resolution of the imaging system. Using the derivative of the Langevin function, we can show that the spatial resolution of MPI is

$$\Delta x \approx 4\frac{H_{sat}}{G} = \frac{24 k_B T}{\mu_0 \pi M_{sat} d^3 G} \tag{4}$$

where Δx is the full-width at half-maximum (FWHM) of the PSF (See Figure 1(b)). Here, M_{sat} [A/m] is the saturation magnetization of the nanoparticles, d [m] is the nanoparticle diameter, k_B is Boltzmann's constant, T is the temperature, and μ_0 is the vacuum permeability.

We have proven both experimentally[2] and theoretically[17] that X-space MPI produces images that are both Linear and Shift

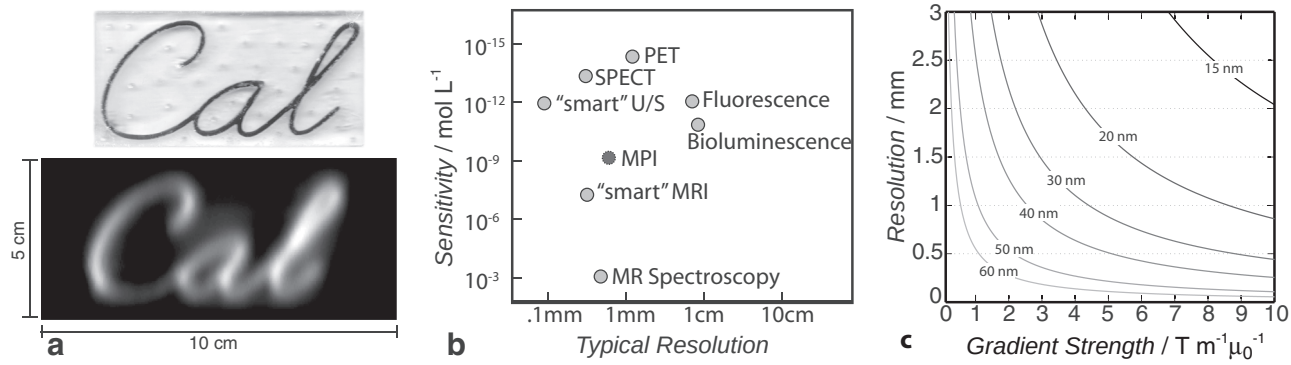

Figure 2. (a) The MPI technique has incredible contrast and only sees tracer. Shown here is an Acrylic phantom containing diluted Resovist tracer (1 part Resovist, 9 parts water) and the corresponding native X-space MPI scan of the phantom taken using the Berkeley FFL scanner (See Figure 4). Total acquisition time of 8 seconds. Native Resolution of 3.8 mm. (b) The sensitivity and resolution of MPI compare well with other pre-clinical imaging techniques for use in small animals. "Smart" U/S and "smart" MRI refer to the use of tracers such as microbubbles and Gadolinium/SPIO nanoparticles, respectively. Chart adapted from Meikle et. al. 2005.[18] (c) The theoretical resolution of MPI by nanoparticle diameter and gradient strength. Our current UC Berkeley scanners have gradient strengths that vary from 2.35 T $m^{-1}\mu_0^{-1}$ to 6 T $m^{-1}\mu_0^{-1}$.

Invariant (LSI). LSI properties are not guaranteed in an imaging system, but are crucial for quantitative imaging. Fortunately, most imaging techniques are approximately LSI, including CT, MRI, Ultrasound, and PET/SPECT. The most notable techniques that are not LSI include planar X-ray imaging and optical fluorescence/bioluminescence imaging in small animals. To linearize X-ray imaging and enable CT, for example, we reconstruct the logarithm of the signal to form an image in Hounsfield units. Similarly, to enable LSI in x-space MPI, we must velocity compensate the received signal and recover lost low-frequency information due to filtering. Following x-space reconstruction, the MPI signal is perfectly linear with quantity of iron oxide nanoparticles ($R^2 = 0.99$) and shift invariant.

3. MPI Fundamentals: Contrast, Sensitivity and Resolution

X-space MPI allows us to predict how MPI will compare to other imaging modalities when it comes to the most fundamental imaging parameters: contrast, resolution, and sensitivity. In **Figure 2**(a) we see the ideal contrast of MPI in imaging a "Cal" phantom, which shows the tracer with no confounding background signal. In Figure 2(b) we see an overall comparison of the resolution and sensitivity of MPI and the dominant pre-clinical imaging modalities (adapted from Meikle *et. al.* 2005).[18] The millimeter-scale resolution of MPI sets it apart from fluorescence and bioluminescence imaging in small animals, as optical imaging in tissue thicker than a few millimeters has resolution approaching a centimeter. For full-body imaging techniques with resolution independent of depth, MPI could theoretically achieve the highest sensitivity without requiring radioactive tracers.

3.1. Contrast

The MPI technique has ideal contrast for visualizing iron oxide tracers. MPI does not see tissue whatsoever, and so the contrast is similar to nuclear medicine for detecting a tracer with minimal background. Since the MPI technique sees the tracer with exceptional fidelity, the contrast of the technique is instead defined by the efficacy of the tracer for the physiological process being investigated. For example, MPI is near-ideal for angiography because the tracer is safe to inject and it is possible to engineer SPIO nanoparticles to have hours of circulation time. However, large-diameter nanoparticles are quickly filtered from the bloodstream by Kupffer cells in the liver. It will be important to minimize the hydrodynamic diameter of the SPIOs with innovative thin coatings, which are essential to prevent aggregation of the particles.

3.2. Sensitivity/SNR

The physics of MPI's SNR predict that MPI could soon approach 20 nanomolar sensitivity.[1,3] This is very promising considering the FDA safety studies on Ferumoxytol showing that even CKD patients can safely tolerate 2 millimolar SPIO concentrations.[11] For perspective, MPI's theoretical sensitivity is better than MRI when detecting gadolinium tracer (~50 micromolar detection limit).[19] We believe this remarkable sensitivity limit would enable new biological experiments, even approaching quantitative single-cell imaging inside a live animal.

At present, the lack of optimized tracers and the current state of MPI hardware both limit the achievable sensitivity of MPI. The most commonly used tracer, Resovist, is not optimized for MPI and it is estimated that only 3% of Resovist contributes to the MPI signal.[1,20] This is in contrast to tailored tracers being developed, such as the tracer shown in **Figure 3**(b), where nearly 100% of the sample contributes to the signal. MPI is also still in the early steps of the engineering effort needed to reach the physical limits of the technique. This can be contrasted to MRI, where engineers have used the decades since its invention to optimize scanners to the point where the patient is the dominant noise source; further RF coil improvements are of little SNR benefit in MRI. In MPI, no research group has yet reduced interference and coil noise to that level. Hence, we believe hardware and nanoparticle research efforts could dramatically improve the sensitivity of real-world MPI scanners.

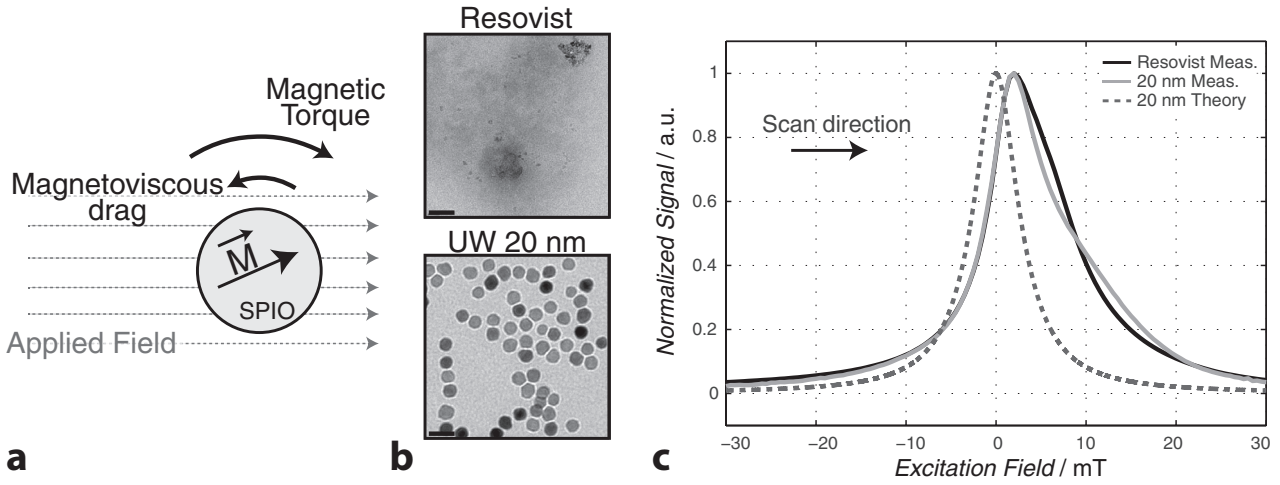

Figure 3. (a) The ability of a magnetic nanoparticle to rotate to follow an applied field and produce a MPI signal is impeded by magnetoviscous drag. (b) TEM images of a commercially available contrast agent, Resovist, and tailored nanoparticles with 20 nm mean diameter synthesized at the University of Washington (Scale bars = 40 nm).[21] These TEM images show that we can achieve control on the size and characteristics of the tailored nanoparticles. (c) Measured point spread function using x-space MPI relaxometry.[5] These tailored nanoparticles are already performing on par with Resovist as demonstrated by the measured PSFs, but with significantly improved signal when using the same amount of iron.[20] When compared to the theoretical PSF for 20 nm nanoparticles (dashed line), both measured PSFs demonstrate distortion and lagging due to relaxation effects.[5]

3.3. Resolution

We believe that the biggest hurdle MPI faces today is the poor spatial resolution of current MPI scanners. As discussed above, MPI resolution is fundamentally governed by the gradient strength and the nanoparticle properties. The FWHM resolution given in Equation 4 becomes finer with increasing gradient G and increasing d^3.[3,12] Therefore, neglecting relaxation effects, the resolution in MPI improves with the inverse of the magnetic field gradient strength and cubically with increasing nanoparticle magnetic core diameter, as illustrated in Figure 2(c). Our scanners indicate that Resovist produces a signal similar to a magnetic nanoparticle with 17 ± 4 nm diameter,[2,5] which corresponds to a native resolution of approximately 3.5 mm in a 2.35 T/m gradient. Unfortunately, this resolution is poor when compared with sub-millimeter resolutions (See Figure 2(b)) obtained in the latest generations of PET/SPECT scanners, and 100-micrometer resolution routinely achieved in small animal MRI. To this end, we are targeting a gradient strength of 10 T/m in our next generation scanner, which should allow sub-millimeter resolutions with no change in tracer. We are also working with magnetic nanoparticle experts at the University of Washington to develop SPIOs optimized for MPI.[20,21] Given the theoretical cubic dependence on spatial resolution to particle size, we hope to double spatial resolution by increasing the nanoparticle diameter just 25%, from 17 nm to 22 nm.

4. Optimal Nanoparticle Characteristics for X-space MPI

The relaxation characteristics and magnetic core diameter of the nanoparticle tracer limit the sensitivity and resolution of the MPI technique. Here we explore both the effects of nanoparticle relaxation on MPI images as well as the tradeoffs in tracer design that can result in improved images.

4.1. Relaxation Effects in MPI

Relaxation effects are one of the primary limits to the achievable resolution of the MPI technique. One of the assumptions in x-space MPI theory is that magnetic nanoparticles react instantaneously to the applied field. This is not strictly true as large nanoparticles flip 180° in a fluid slower than small particles. Essentially, viscous drag slows the larger particles (See Figure 3(a)). This relaxation is often called Néel, Brownian, or magneto-viscous relaxation, depending on magnetic domain size, particle size, scan parameters, and coating materials. It is crucial to characterize the time constant for this relaxation, because it effectively reduces the spatial resolution of MPI by blurring the image along the scan direction.

We have devised a technique, x-space MPI relaxometry, to directly measure the crucial parameters of spatial resolution and relaxation times of magnetic nanoparticles by imaging nanoparticles with a virtual gradient field applied using a strong electromagnet.[5] In Figure 3(b) we see a TEM image of Resovist tracer compared with a monodisperse MPI tracer synthesized at the University of Washington. In Figure 3(c), we show experimental data from the X-space relaxometer that shows how the relaxation reduces the achievable resolution by blurring the resulting PSF along the scan direction. We have found that this viscous drag can be effectively modeled with a first-order relaxation time constant, where the real magnetization lags the applied field. Fortunately, we believe this time constant can be reduced through careful magnetic nanoparticle design.

4.2. Optimal Nanoparticles for MPI

Optimizing magnetic nanoparticles expressly for MPI is already emerging as a powerful and exciting area of research in MPI and will be critical for improved sensitivity and improved spatial resolution.[20,21]

As discussed above, resolution improves cubically with nanoparticle diameter. We believe that the optimal resolution should occur for the largest SPIO nanocrystals with a diameter just below the ferromagnetic limit. However, as discussed above, although larger nanoparticles theoretically have the best resolution, their achievable resolution is limited by their relaxation characteristics. To minimize relaxation effects, the nanoparticle's coating size should be minimized. Another concern is that larger nanoparticles, usually dominated by coating size, are known to be taken up in the liver more rapidly than smaller particles. The reduced blood circulation time could limit scan time.

Optimizing a nanoparticle tracer for sensitivity results in considerably different nanoparticles than optimizing for resolution. For optimal sensitivity, a nanoparticle's magnetic moment should immediately rotate to follow the applied magnetic field without requiring physical rotation of the nanoparticle, a process that occurs for nanoparticles dominated by Néel relaxation. For optimal resolution, we need larger nanoparticles, which in turn may experience magneto-viscous relaxation. The process of magneto-viscous relaxation only occurs in particles whose magnetic moment is effectively blocked at the 10's of kHz scanning rates used in MPI, and results in lower signal per unit quantity of iron. This transition from Néel to magneto-viscous relaxation occurs at about 15 nm for round, iron-oxide nanocrystals.[20]

The nanoparticle size dispersion also affects the resulting MPI images. Because nanoparticles move in synchrony with the applied magnetic field, their MPI signals add irrespective of the size distribution of magnetic nanoparticles present. So, nanoparticle tracers can be composed of a wide distribution of nanoparticle diameters and still produce a coherent, focused image. However, the presence of smaller diameter nanoparticles with lower resolution can add a considerable background to the MPI image, reducing both resolution and contrast. Thus, a nanoparticle size distribution should be monodisperse for optimal resolution and contrast.

Preliminary data, theory and simulations predict that nanoparticles optimized for MPI will require a large, monodisperse, single-domain core (approaching 30 nm diameter) for high resolution and a very thin coating to minimize relaxation times and extend circulation time.

5. Current Research Efforts in MPI

The nascent field of MPI offers exciting research avenues for experts in hardware design, image reconstruction, and in medical imaging applications. Below we highlight some of these research avenues.

5.1. Real-time MPI

Very recently, the first 3D real-time MPI images of mice and rats have been acquired with spatial and temporal resolutions sufficient to resolve major organs and vasculature.[13,22] It is important to note that the vascular structures in mice and rats are considerably smaller than the smallest coronary arteries in humans. Furthermore, these small animals have much faster heart rates than humans, so high temporal resolution is essential. The first in vivo demonstration of MPI was performed as a 3D real-time scan (21.5 ms temporal resolution) of a beating mouse heart using 20 μL diluted Resovist injected into the tail vein.[13] Because the circulation time in a mouse is very short (5-10 seconds), high-speed scanning is essential to resolve the tracer flowing through the living mouse.

5.2. Projection MPI

With the aim of eventually reaching real-time 2D frame-rates in humans (akin to X-ray fluoroscopy), we recently built the world's first Projection MPI scanner (See **Figure 4**(a,b)).[6] This scanner is simple in concept, and produces a projection image by using a Field Free Line (FFL), which is a FFP stretched along one axis.[23] The signal that is produced is the integral of the SPIO signal along the FFL. Note that this would be extremely challenging in MRI due to B0 inhomogeneity, but in MPI the frequency-locked rotation of the SPIOs within the entire body ensures no loss of signal coherence even deep within a human.

We have demonstrated that a projection configuration can provide a significant improvement in the imaging speed of MPI. This 2D format allows for much faster imaging, since we need not scan through the third dimension. For example, with 128^3 3D matrix size, a projection scanner could either allow for speedup by a factor of 128 or an SNR boost of $\sqrt{128}$. The projection scanner also enables a much higher-SNR 3D images by rotating the projection plane and reconstructing a 3D volume through projection-reconstruction.[6,24]

Some of our most recent small animal images acquired with our projection scanner are shown in Figures 4(c,d). These MPI images show the biodistribution of SPIO nanoparticle tracers in a mouse, with contrast superior to MRI, and with resolution that already surpasses whole-body optical imaging. These MPI projection scans of mice were acquired after tail vein injection with 20 μL (556 μg Fe) of undiluted Resovist tracer. The first mouse was sacrificed 30 seconds after injection, whereas the second mouse was sacrificed 5 minutes after injection. Both mice were imaged after sacrifice. Note that in Figure 4(c), the tracer in the early phase extends to the brain, heart, and liver. In the later stages in Figure 4(d), it is apparent that the Resovist tracer is rapidly filtered from the blood stream and is concentrated in the liver. The MRI anatomic reference scan (taken post-sacrifice) shows a dark liver, demonstrating that Resovist (a T_2* agent) has already accumulated in the liver.

6. Future of MPI

MPI is perhaps the first imaging technique since MRI that can be scaled up easily to imaging deep within humans, and we believe it offers extraordinary promise as an emerging medical imaging modality. Significant work remains until MPI can become clinically relevant, particularly with regards to synthesizing ideal magnetic nanoparticle tracers, building new

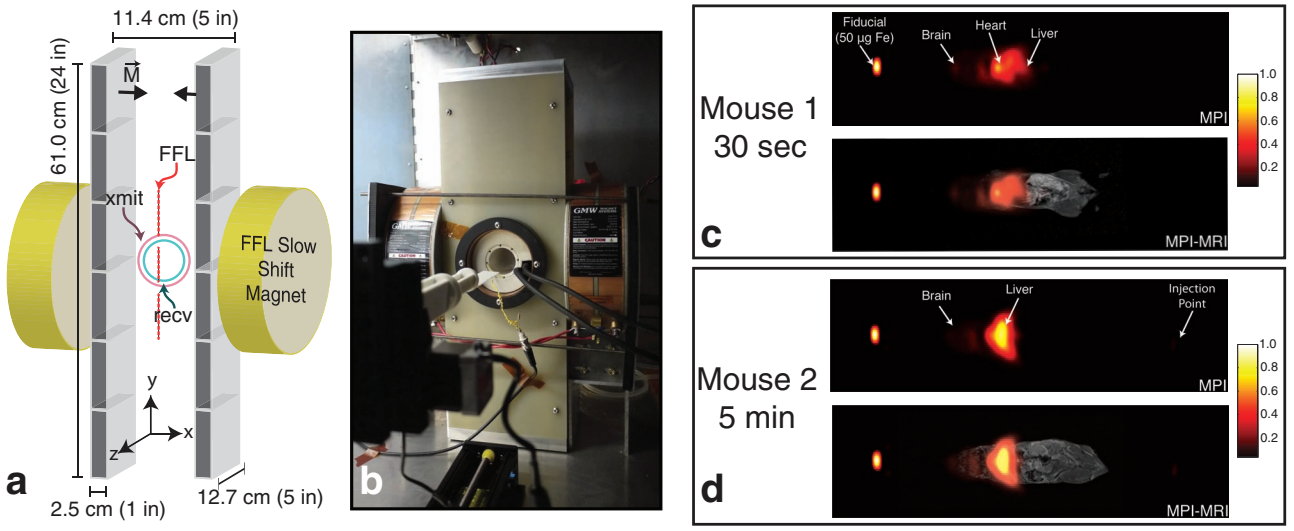

Figure 4. Berkeley Projection MPI scanner and Full-body X-space MPI projection scans of mice. (a) Schematic of the Berkeley Projection MPI scanner. The Projection image occurs in the up/down direction (red-dashed line) and is produced using a Field Free Line (FFL). The FFL is formed by clusters of permanent magnets facing each other. (b) Photograph of the projection MPI scanner as built. (c) Full-body MPI projection scan of a mouse injected in a tail vein with 20 µL (556 µg Fe) undiluted Resovist tracer and sacrificed after 30 seconds. The resulting MPI image shows an MPI-MRI visible fiducial (50 µg Fe, scaled to signal value of 1.0), as well as the outlines of the mouse brain, heart, and liver. (d) Full-body MPI projection scan of an identically prepared mouse, but with a pause of 5 minutes after injection and before sacrifice. In the projection MPI scan, it is apparent that the Resovist tracer is rapidly filtered from the blood stream by the liver. The MRI scan (taken post-sacrifice) shows a dark liver as Resovist is a T_2* agent. MPI FOV = 6 cm x 20 cm. Native Resolution of 3.8 mm.

generations of MPI scanning hardware and developing new scanning methodologies. Fortunately, we see no fundamental hardware limitation that would prevent scaling MPI up to human sizes. A human MPI scanner would require either much heavier permanent magnet gradient or a superconducting gradient. A superconducting gradient would put system costs and complexity similar to that of a modern 1.5 T superconducting MRI scanner. Numerous groups are developing some of the first pre-clinical imagers but there is, at present, no commercially available scanner.

We believe that MPI will find its place in rapid angiography, cancer detection and cell therapy tracking. Early adoption is likely to occur for the Chronic Kidney Disease (CKD) patient population, who have no safe angiography alternative.

In addition to angiographic applications, there has been significant interest in using MPI for detecting tagged cells in vivo. It is straightforward to label cells with iron oxide nanoparticles.[25] The magnetic tags are non-toxic, remain stable for weeks in vivo, and do not alter cell function. MPI would be ideal for imaging the distribution of cellular therapy agents quantitatively at any depth in an animal.

Another exciting direction for future MPI research is the field of cancer detection. For revealing early stage cancer with MPI, we require a magnetic nanoparticle that exploits the enhanced permeability and retention of tumors.[26] MPI would also be ideal for imaging magnetic nanoparticles functionalized to sense, seek out and linger in tumors. Here, we can quickly transfer the enormous research efforts in functionalized magnetic nanoparticles developed for MRI cancer imaging. This is especially promising for vascular inflammation targets such as atherosclerotic plaques and cancers.[27]

Acknowledgements

P Goodwill and E Saritas contributed equally to this work. This work was supported in part by CIRM Tools and Technology Grant RT1-01055-1, and a UC Discovery grant. The contents of this publication are solely the responsibility of the authors and do not necessarily represent the official views of CIRM or any other agency of the State of California. This work was supported in part by Grant Number 1R01EB013689 from the National Institute of Biomedical Imaging and Bioengineering. The content is solely the responsibility of the authors and does not necessarily represent the official views of the National Institute of Biomedical Imaging and Bioengineering or the National Institutes of Health.

Published online: March 19, 2012

[1] B. Gleich, J. Weizenecker, *Nature* **2005**, *435*, 1214.
[2] P. W. Goodwill, S. M. Conolly, *IEEE T. Med. Imaging* **2011**, *30*, 1581.
[3] P. W. Goodwill, S. M. Conolly, *IEEE T. Med. Imaging* **2010**, *29*, 1851.
[4] P. W. Goodwill, G. C. Scott, P. P. Stang, S. M. Conolly, *IEEE T. Med. Imaging* **2009**, *28*, 1231.
[5] P. W. Goodwill, A. Tamrazian, L. R. Croft, C. D. Lu, E. M. Johnson, R. Pidaparthi, R. M. Ferguson, A. P. Khandhar, K. M. Krishnan, S. M. Conolly, *Appl. Phys. Lett.* **2011**, *98*, 262502.
[6] P. W. Goodwill, J. J. Konkle, B. Zheng, E. U. Saritas, S. M. Conolly, *IEEE T. Med. Imaging* **2012**, (in press).
[7] R. W. Katzberg, C. Haller, *Kidney Int. Supp.* **2006**, S3.
[8] P. A. McCullough, *J. Am. Coll. Cardiol.* **2008**, *51*, 1419.
[9] P. H. Kuo, E. Kanal, A. K. Abu-Alfa, S. E. Cowper, *Radiology* **2007**, *242*, 647.
[10] J. H. Ix, N. Mercado, M. G. Shlipak, P. A. Lemos, E. Boersma, W. Lindeboom, W. W. O'Neill, W. Wijns, P. W. Serruys, *Am. Heart J.* **2005**, *149*, 512.

[11] M. Lu, M. H. Cohen, D. Rieves, R. Pazdur, *Am. J. Hematol.* **2010**, *85*, 315.
[12] J. Rahmer, J. Weizenecker, B. Gleich, J. Borgert, *BMC Med. Imaging* **2009**, *9*, 4.
[13] J. Weizenecker, B. Gleich, J. Rahmer, H. Dahnke, J. Borgert, *Phys. Med. Biol.* **2009**, *54*, L1.
[14] A. M. Rauwerdink, J. B. Weaver, *Med. Phys.* **2010**, *37*, 2587.
[15] D. B. Twieg, *Med. Phys.* **1983**, *10*, 610.
[16] T. Knopp, S. Biederer, T. F. Sattel, M. Erbe, T. M. Buzug, *IEEE T. Med. Imaging* **2011**, *30*, 1284.
[17] K. Lu, P. W. Goodwill, B. Zheng, S. M. Conolly, in *Proc. SPIE 7965*, **2011**, 79652I.
[18] S. R. Meikle, P. Kench, M. Kassiou, R. B. Banati, *Phys. Med. Biol.* **2005**, *50*, R45.
[19] V. Jacques, J. Desreux, in *Contrast Agents I* vol. *221* (Ed: W. Krause), Springer Berlin/ Heidelberg, **2002**, pg. 123.
[20] R. M. Ferguson, K. R. Minard, A. P. Khandhar, K. M. Krishnan, *Med. Phys.* **2011**, *38*, 1619.
[21] R. M. Ferguson, K. R. Minard, K. M. Krishnan, *J. Magn. Magn. Mater.* **2009**, *321*, 1548.
[22] I. Schmale, J. Rahmer, B. Gleich, J. Kanzenbach, J. D. Schmidt, C. Bontus, O. Woywode, J. Borgert, in *Proc. SPIE 7965*, **2011**, 796510.
[23] J. Weizenecker, B. Gleich, J. Borgert, *J. Phys. D: Appl. Phys.* **2008**, 41.
[24] T. Knopp, T. F. Sattel, S. Biederer, T. M. Buzug, *J. Phys. A: Math. Theor.* **2010**, *43*, 012002.
[25] A. S. Arbab, G. T. Yocum, H. Kalish, E. K. Jordan, S. A. Anderson, A. Y. Khakoo, E. J. Read, J. a. Frank, *Blood* **2004**, *104*, 1217.
[26] T. Barrett, M. Brechbiel, M. Bernardo, P. L. Choyke, *J. Magn. Reson. Im.* **2007**, *26*, 235.
[27] D. Simberg, T. Duza, J. H. Park, M. Essler, J. Pilch, L. Zhang, A. M. Derfus, M. Yang, R. M. Hoffman, S. Bhatia, M. J. Sailor, E. Ruoslahti, *Proc. Natl. Acad. Sci. USA* **2007**, *104*, 932.